Chemical Geology 644 (2024) 121831

Contents lists available at ScienceDirect

Chemical Geology

journal homepage: www.elsevier.com/locate/chemgeo

Phosphate oxygen isotopes constrain Mesoproterozoic marine temperatures and the paucity of phosphorite

Yuntao Ye [a,b], Xiaomei Wang [b], Huajian Wang [b], Haifeng Fan [c,d], Zhigang Chen [e], Qingjun Guo [d,f], Ziteng Wang [d,f], Chaodong Wu [a], Donald E. Canfield [b,g], Shuichang Zhang [b,*]

[a] Key Laboratory of Orogenic Belts and Crustal Evolution, Ministry of Education, School of Earth and Space Sciences, Peking University, Beijing 100871, China
[b] Key Laboratory of Petroleum Geochemistry, Research Institute of Petroleum Exploration and Development, China National Petroleum Corporation, Beijing 100083, China
[c] State Key Laboratory of Ore Deposit Geochemistry, Institute of Geochemistry, Chinese Academy of Sciences, Guiyang 550081, China
[d] University of Chinese Academy of Sciences, Beijing 100049, China
[e] College of Ocean and Earth Sciences, Xiamen University, Xiamen 361102, China
[f] Institute of Geographic Sciences and Natural Resources Research, Chinese Academy of Sciences, Beijing 100101, China
[g] Nordcee, Department of Biology, University of Southern Denmark, 5230 Odense, Denmark

ARTICLE INFO

Editor: Hailiang Dong

Keywords:
Apatite
Phosphate oxygen isotopes
Gaoyuzhuang formation
Xiamaling formation
North China

ABSTRACT

Phosphorus (P) is an essential element for life, and the oceanic P cycle is closely coupled with the global carbon and oxygen cycles via the role of P as a limiting nutrient. Since P has only one stable isotope, tracking the P cycle through geological history is challenging. However, phosphate oxygen isotopes ($\delta^{18}O_p$) represent a valuable tool for deciphering various P-related reactions, such as intracellular P turnover and enzymatic P regeneration, and have been successfully applied to modern soils and marine sediments. The marine P cycle prior to the Neoproterozoic Era remains controversial due to the scarcity of phosphorite and large uncertainties in estimating seawater phosphate levels. Here, we present $\delta^{18}O_p$ of carbonate fluorapatite (CFA) from the Mesoproterozoic Gaoyuzhuang and Xiamaling Formations in North China. Despite considerable uncertainties, the derived authigenic $\delta^{18}O_p$ values are markedly lower than those from modern sites with similar depth and latitude, which imply a warmer climate during the Mesoproterozoic Era compared to the present day. Based on thermodynamic calculations of saturation state with respect to CFA, we suggest that the elevated temperatures could have hindered P authigenesis, partially accounting for the general absence of phosphorite in contemporaneous successions.

1. Introduction

Phosphorus (P) plays wide-ranging roles in cell structure and function and is required for the growth of all organisms. Phosphorus availability can affect rates of photosynthesis, a process through which oxygen is produced and newly fixed carbon is sequestered from the atmosphere into the deep oceans. Therefore, the P cycle is important in regulating the global biogeochemical cycles of carbon and oxygen (e.g., Van Cappellen and Ingall, 1996; Algeo and Ingall, 2007; Walton et al., 2023). In general, marine phosphate levels are controlled by the interplay between P sources and sinks. Terrestrial weathering is the primary agent for transporting P into the modern oceans, while in anoxic settings, as for Precambrian oceans, alteration of submarine basalts may also provide considerable amounts of P (Syverson et al., 2021). The dominant sink for seawater P is deposition and burial in marine sediments, and when P is strongly enriched (P_2O_5 > 15–20 wt%), deposits are known as phosphorite. Strikingly, phosphorite intermittently occurred during the Phanerozoic Eon, but is remarkably rare before the Neoproterozoic Era, with the only exception of the Paleoproterozoic phosphogenesis event (Papineau, 2010).

The paucity of phosphorite and the generally low P abundance in shales from the Archean Eon and the Mesoproterozoic Era have spawned the idea that marine P reservoirs were much smaller when compared with the Neoproterozoic (Reinhard et al., 2017; Planavsky et al., 2023). Limited P availability during the Archean Eon is consistent with reconstructions based on P/Fe ratios in iron oxides (Bjerrum and Canfield,

* Corresponding author.
E-mail address: sczhang@petrochina.com.cn (S. Zhang).

https://doi.org/10.1016/j.chemgeo.2023.121831
Received 8 May 2023; Received in revised form 6 November 2023; Accepted 15 November 2023
Available online 19 November 2023

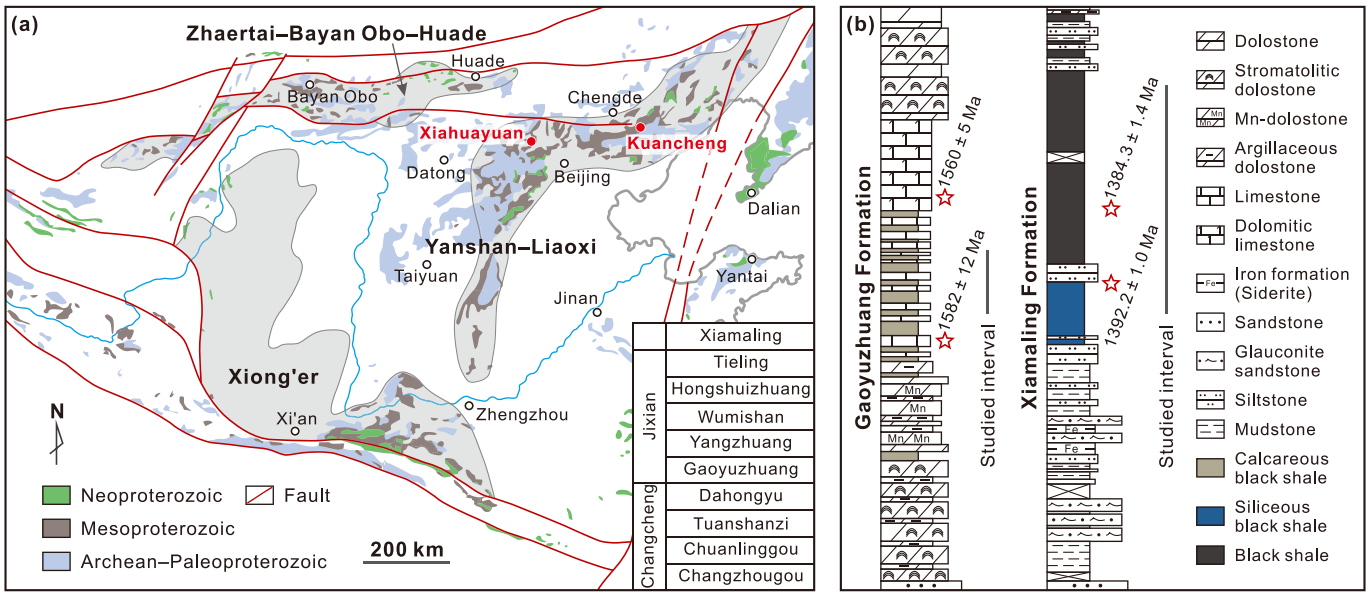

Fig. 1. Geological map of North China (a) and stratigraphic columns of the Gaoyuzhuang and Xiamaling Formations (b). Locations of the studied drill cores are marked as red dots. Age data sources: Li et al., 2010; Zhang et al., 2015; Tian et al., 2020. (For interpretation of the references to colour in this figure legend, the reader is referred to the web version of this article.)

2002; Jones et al., 2015). It is speculated that under predominately ferruginous conditions, P could have been effectively removed from seawater via the formation of ferrous phosphate minerals (e.g., vivianite), and co-precipitation or adsorption with iron-bearing particles, leading to a severe P crisis with high C/P ratios in marine biomass (Reinhard et al., 2017).

In contrast, other evidence has pointed to abundant P in Precambrian oceans. For examples, measurements of carbonate-associated phosphate suggested that dissolved P in Archean oceans were 4–12 times higher than today (Ingalls et al., 2022; but see Crockford and Halevy, 2022 for an alternative interpretation). The direct precipitation of apatite from Archean hydrothermal vents would require 5–50 times higher P concentrations in the deep waters relative to the modern (Rasmussen et al., 2021). Furthermore, an integrated study of Mesoproterozoic-aged sediments revealed no enhanced P removal under ferruginous conditions compared to oxic and euxinic counterparts (Canfield et al., 2020), weakening the role of ferruginous sediments as a significant P sink.

A critical constraint in quantifying the ancient P cycle is a lack of inherent tracer. Since P has only one stable isotope (^{31}P), it cannot be used to monitor P systematics in a similar manner to other essential elements. Alternatively, most P in marine systems is tightly bound to oxygen, permitting the analysis of oxygen stable isotopes ($\delta^{18}O_p$) as a valuable complement for tracking the P cycle (e.g., Longinelli and Nuti, 1968; Colman et al., 2005; Blake et al., 2010; McLaughlin et al., 2013). The P—O bound in dissolved phosphate does not exchange oxygen with ambient fluid under abiotic conditions at Earth's surface temperature and pH ranges (Chang et al., 2021). However, significant exchange of oxygen isotopes between phosphate and water occurs through enzymatic activity when P is decomposed from organic matter or when P is cycled intracellularly (Davies et al., 2014). In the latter case, the biological turnover of P drives phosphate to approach oxygen isotope equilibrium with surrounding medium at the temperature of the reaction. The major enzyme that catalyzes this process is inorganic pyrophosphatase, a ubiquitous enzyme found in all life forms (Blake et al., 2005).

Apatite, a major P host in sediments, was proved to possess negligible fractionation (~1‰ VSMOW) in $\delta^{18}O_p$ between aqueous- and solid-phase phosphate (Liang and Blake, 2007), which can therefore be used as a carrier of ancient $\delta^{18}O_p$ signatures. If the dissolved phosphate from which the apatite is precipitated is in equilibrium with the ambient water, the $\delta^{18}O_p$ of apatite should reflect its formation temperature. This oxygen isotope thermometry can be written as (Lécuyer et al., 2013):

$$T = 117.4 \pm 9.5 - (4.5 \pm 0.43) \times \left(\delta^{18}O_p - \delta^{18}O_w\right) \quad (1)$$

where T denotes the temperature in degrees Celsius and $\delta^{18}O_w$ is the oxygen isotopes of water.

Phosphate oxygen isotopes of apatite preserved in modern soils and sediments have been utilized to reconstruct temperatures, with results both in equilibrium and disequilibrium with waters (Shemesh et al., 1988; Jaisi and Blake, 2010; Tamburini et al., 2012; Zhao et al., 2021). Exploring the application of $\delta^{18}O_p$ to geological archives is a worthwhile endeavor. Here, we report apatite clusters from the Mesoproterozoic Gaoyuzhuang (~1.57 Ga) and Xiamaling (~1.4 Ga) Formations in North China. Through $\delta^{18}O_p$ analysis, we attempt to estimate Mesoproterozoic pore water temperatures and discuss their impact on P authigenesis, which might explain the general absence of phosphorite during the Mesoproterozoic Era.

2. Geological setting and samples

Thick Proterozoic successions were developed on the North China Craton. The Yanshan–Liaoxi (Yanliao) Basin in particular has a well-established Proterozoic stratigraphy that offers a solid foundation for geochemical investigation (Fig. 1a; Zhai et al., 2014; Li et al., 2019). The Changzhougou Formation, the oldest of the Proterozoic sediment package in the Yanliao Basin, is made up of conglomerates and sandstones, representing littoral deposition with fluvial and alluvial influences. The overlying Chuanlinggou Formation consists of sandstones and mudstones, which were deposited during basin deepening. These siliciclastics pass into dolostones of the Tuanshanzi Formation, indicative of shallow marine carbonate platform environment. Moving upward, abundant volcanoclastics characterize the Dahongyu Formation.

The Gaoyuzhuang Formation, the beginning of the Jixian System, is typified by thick-bedded stromatolitic dolostones, while subordinate Mn-bearing dolostones and shales occur in the lower and middle portions of this formation. It is believed that the widespread distribution of the Gaoyuzhuang carbonates marks a transition from active to passive margin setting (Qu et al., 2014). The Yangzhuang Formation, composed of muddy dolostones, is interpreted to have been deposited in inter- and

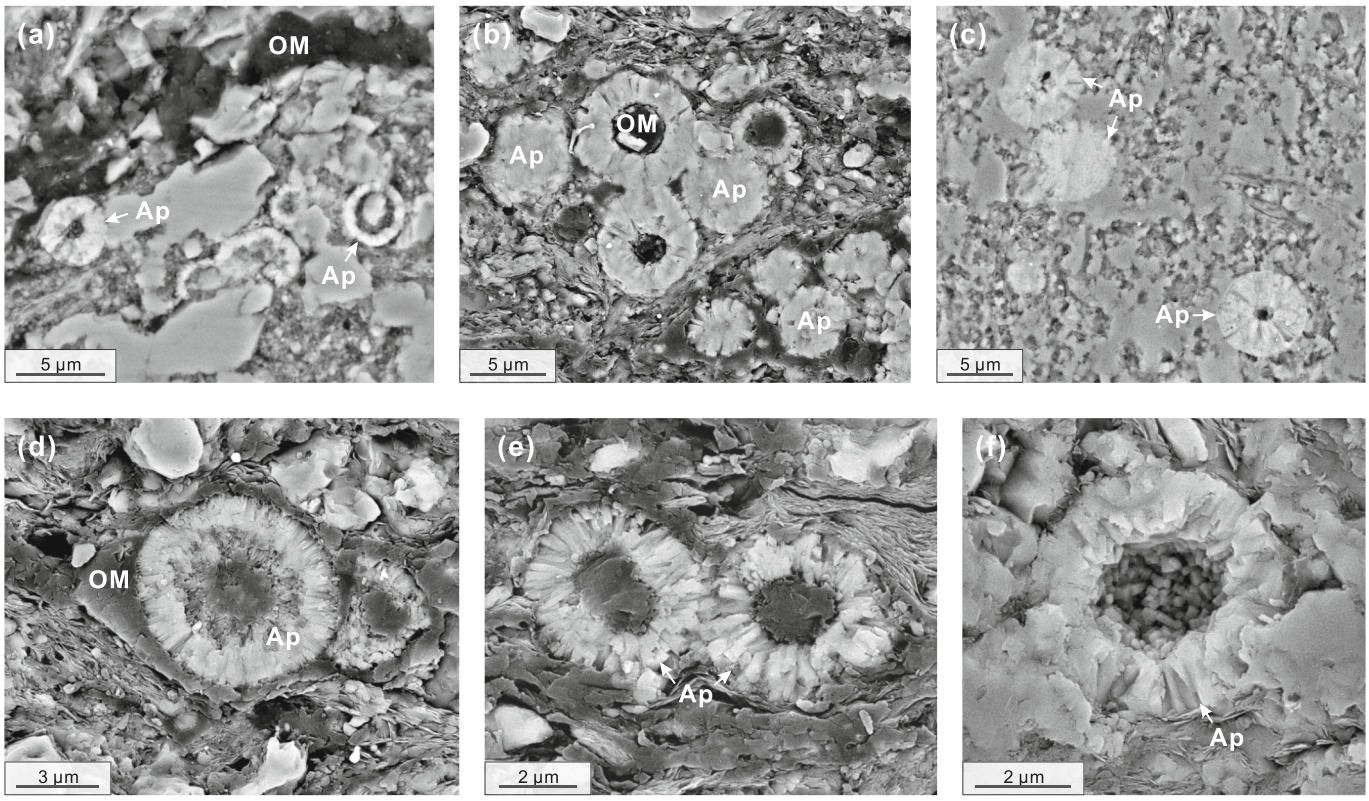

Fig. 2. SEM images of apatite preserved in the Gaoyuzhuang and Xiamaling Formations. Ap, apatite; OM, organic matter. See text for details.

super-tidal zones, giving way to monotonous dolostones of the Wumishan Formation, and black shales of the Hongshuizhuang Formation through relative sea level rise. Subsequent shoaling resulted in the deposition of the Tieling carbonates and the flourishing of stromatolites. Sediments overlying the Tieling Formation are conglomerates and sandstones of the Xiamling Formation, finning upward into siltstones and shales (Meng et al., 2011; Wang et al., 2017).

Our samples are shales of the Gaoyuzhuang and Xiamaling Formations (Fig. 1b). In recent years, great progress has been made in the chronostratigraphy of these two formations. Tuff layers in the middle of the Gaoyuzhuang Formation have zircon U—Pb ages of 1582 ± 12 (Tian et al., 2020), 1560 ± 5, and 1559 ± 12 Ma (Li et al., 2010). The Xiamaling Formation, which was once assigned to the Neoproterozoic Era, is now firmly established as Mesoproterozoic with zircon U—Pb ages of 1392.2 ± 1.0, 1384.3 ± 1.4 (Zhang et al., 2015), 1380 ± 36, 1379 ± 12 (Su et al., 2008), 1372 ± 18 (Su et al., 2010), 1370 ± 11 (Gao et al., 2008b), 1368 ± 12 (Gao et al., 2007), and 1366 ± 9 Ma (Gao et al., 2008a). Paleomagnetism place the North China Craton at low-latitude during the Mesoproterozoic Era (Zhang et al., 2012, 2021). Drill cores capturing the Gaoyuzhuang and Xiamaling rocks were recovered in the Kuancheng and Xiahuayuan areas, respectively. The lack of storm wave imprint in the selected shales suggests a water depth of >100–200 m (Stow et al., 2001). Detailed descriptions of sedimentology and chemostratigraphy are given elsewhere (Wang et al., 2017; Ye et al., 2021, 2023).

3. Methods

Thin sections were employed for mineralogical observations with a Thermo Fisher Scientific Apreo scanning electron microscope (SEM) at the Key Laboratory of Petroleum Geochemistry, China National Petroleum Corporation. This instrument is equipped with a Bruker XFlash 6–30 energy dispersive spectrometer (EDS) for elemental composition determination. To improve conductivity, sample was coated with gold before analysis. Backscattered electron images and SEM-EDS data were collected under high vacuum conditions (10 kV and 0.8 nA).

Major elements were acquired at the Analytical Laboratory of Beijing Research Institute of Uranium Geology, China National Nuclear Corporation. In brief, fused discs were prepared in a crucible (95% Pt–5% Au) with 0.7 g of sample, 5.9 g of flux ($Li_2B_4O_7$–LiF–NH_4NO_3), and 1 mL of LiBr, and then melted under 1150–1250 °C for 10–15 min. The discs were analyzed by a PANalytical Axios^{mAX} wavelength dispersive X-ray fluorescence spectrometer. The analytical precision given by replicate tests of shale standards and samples was better than 2%.

Samples enriched in P from the Gaoyuzhuang and Xiamaling Formations were selected for $\delta^{18}O_p$ determination. Phosphate purification was conducted at the College of Ocean and Earth Sciences, Xiamen University, according to the method of Chen et al. (2015) and Lei et al. (2020). Specifically, the sample was extracted with 1 M HCl for 16 h and the supernate was separated from the residue by centrifugation. An aliquot of the supernate was measured for P content by a Thermo Fisher Scientific X Series 2 inductively coupled plasma-mass spectrometer at the Guizhou Tongwei Analytical Technology Co., Ltd. Magnesium-induced co-precipitation was employed to obtain phosphate. The precipitate was re-dissolved with 10 M HNO_3 and purified by precipitation of phosphate as ammonium phosphomolybdate and magnesium ammonium phosphate. After re-dissolution, the solution was treated with cation (AG 50 W-X8, BIO-RAD) first and then anion resins (AG 1-X8, BIO-RAD) to remove interfering ions. Phosphate adsorbed on the anion resin was eluted with 0.2 M $NaHCO_3$. Residual carbonate was removed by adding 7 M HNO_3 and purging with N_2. The purified phosphate was converted to Ag_3PO_4 by ammonia volatilization.

Phosphate oxygen isotope ratios were analyzed by a high-temperature conversion-isotope ratio mass spectrometry (Flash EA 1112 Series, Delta V Advantage, Thermo Fisher Scientific) and reported relative to the VSMOW standard. The measured $\delta^{18}O_p$ compositions were calibrated by the IAEA-601 benzoic acid ($\delta^{18}O_p$ = 23.14‰) and the B2207 silver phosphate ($\delta^{18}O_p$ = 21.7‰, Elemental Microanalysis). The

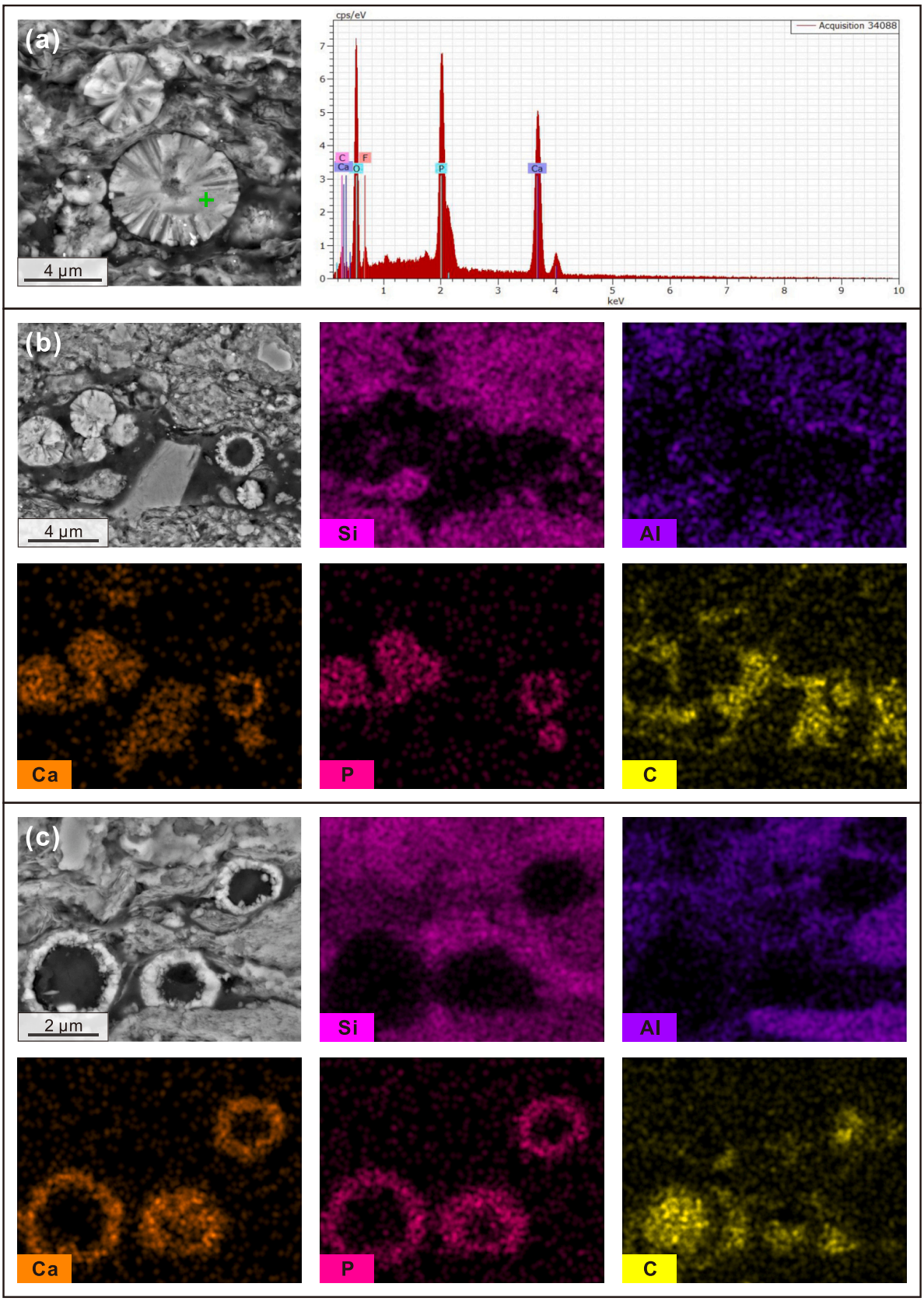

Fig. 3. SEM-EDS results. (a) A typical EDS spectra of apatite. (b–c) EDS maps showing the close association between apatite and organic matter.

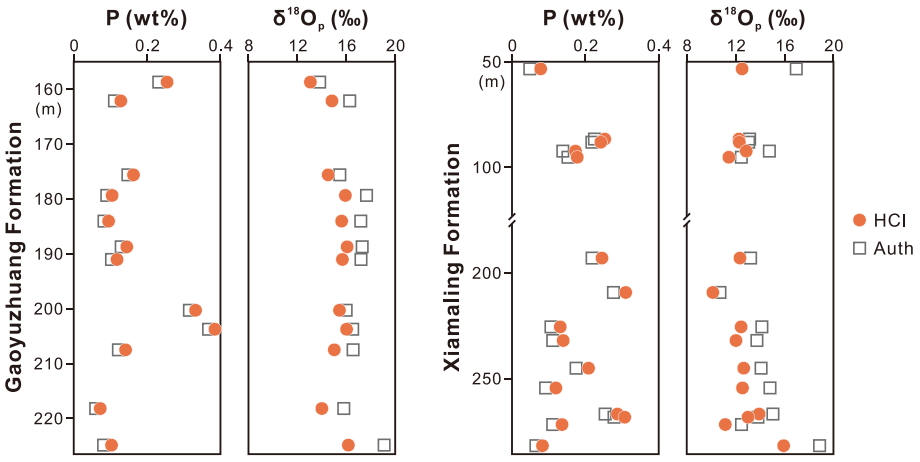

Fig. 4. Geochemical profiles of the Gaoyuzhuang and Xiamaling Formations. Note that the dots represent the P contents and $\delta^{18}O_p$ of the HCl-extractable pool, encompassing both detrital and authigenic (open squares) components.

analytical reproducibility was better than 0.3‰. Parallel $\delta^{18}O_p$ analysis was conducted at the Institute of Geographic Sciences and Natural Resources Research, Chinese Academy of Sciences after the method of Tian et al. (2016). Replicate determinations between the two laboratories agreed within 0.6‰.

4. Results

SEM-EDS analysis reveals the presence of carbonate fluorapatite (CFA) spheroids (~5 μm) in all the examined samples, while in organic-rich laminae CFA often occurs as clustered aggregates (Figs. 2 and 3). The CFA spheroids are not single crystal but consist of tiny apatite particles exhibiting radial features (Fig. 2d–f). The centers of these spheroids are filled with smaller apatite grains (Fig. 2f), sometimes with organic matter (Figs. 2 and 3). Elemental mapping suggests a close relationship between CFA and organic matter. The former is identified by the co-enrichment of Ca and P, while the latter is characterized by carbon enrichment (Fig. 3). However, dispersed CFA globules without clear evidence of organic matter are also observed (Fig. 2c). Geochemical results show that the selected samples are generally enriched in P (P = 0.07–0.42 wt%; Fig. 4) compared to other Mesoproterozoic sediments (P = ~0.03 wt%, the Mesoproterozoic median in the database of Planavsky et al., 2023; Fig. 5). The HCl-extractable $\delta^{18}O_p$ compositions of the Gaoyuzhuang and Xiamaling Formations range from 13.0‰ to 16.1‰ and 10.1‰ to 15.9‰, respectively, with no obvious stratigraphic variation (Fig. 4; Table S1). Notably, these values, together with a compilation of $\delta^{18}O_p$ data from P-bearing rocks, help define an increasing trend in $\delta^{18}O_p$ with decreasing ages (Fig. 5a; Table S2).

5. Discussion

5.1. Authigenic phosphate oxygen isotope compositions

Since the HCl-extractable P pool (P_{HCl}) represents a mixture of authigenic and detrital P, a lithogenic correction is required to determine the $\delta^{18}O_p$ of the authigenic fraction ($\delta^{18}O_{auth}$). The $\delta^{18}O_{auth}$ can be estimated by the following mass balance equations:

$$\delta^{18}O_{auth} = \left(P_{HCl} \times \delta^{18}O_{HCl} - P_{det} \times \delta^{18}O_{det}\right)/\left(P_{HCl} - P_{det}\right) \quad (2)$$

$$P_{det} = (P/Al)_{det} \times Al_{sample} \quad (3)$$

where $\delta^{18}O_{HCl}$ and $\delta^{18}O_{det}$ denote the HCl-extractable and detrital $\delta^{18}O_p$ values, respectively, P_{HCl} is the P content extracted by 1 M HCl, P_{det} is the detrital P abundance, Al_{sample} stands for the bulk Al content in our samples, and $(P/Al)_{det}$ signifies the detrital background.

We evaluate $\delta^{18}O_{det}$ by compiling published igneous apatite $\delta^{18}O_p$ compositions (average = 5.3 ± 2.3‰; Table S3; Conway and Taylor, 1969; Mizota et al., 1992; Tichomirowa et al., 2006; Broom-Fendley et al., 2016; Bruand et al., 2019; Sun et al., 2020; Smith et al., 2021). We note that local inputs of P with higher $\delta^{18}O_{det}$ are plausible due to sedimentary CFA recycling. In general, a higher $\delta^{18}O_{det}$ leads to more ^{18}O-depletion of $\delta^{18}O_{auth}$ and correspondingly a warmer temperature when $\delta^{18}O_{auth}$ was in equilibrium with the ambient solution.

Based on the upper continental crust (UCC) composition (Rudnick and Gao, 2014) and the assumption that reactive P makes up 35% of the total P in UCC, the ratio of $(P/Al)_{det}$ was estimated to be 0.005 (Canfield et al., 2020). The reactive P flux of 35% is the mean of the percentage (25–45%) believed to be associated with riverine particulates (Ruttenberg, 2014). The calculated detrital P pool accounts for a small portion of the entire sedimentary P pool (mostly <20%), which is consistent with sequential extractions of marine sediments (Algeo and Ingall, 2007; Jaisi and Blake, 2010). We stress that our mass balance calculation represents a very rough approximation of $\delta^{18}O_{auth}$. If the true P_{det} concentration is greater than our estimate, the calculated $\delta^{18}O_{auth}$ would be lower than the actual value, and vice versa.

5.2. Constraining Mesoproterozoic marine temperatures

Studies on modern oceans and sediments showed that CFA precipitations take place in the water column or near the sediment–water interface (e.g., Faul et al., 2005; Ruttenberg, 2014). SEM images of our samples reveal deflections of organic-rich or clay laminae around the margins of CFA as well as the co-occurrence of CFA and organic materials (Figs. 2 and 3), indicating an early diagenetic origin for CFA. Indeed, the early diagenetic formation of CFA has been inferred to be mediated by bacteria, which can not only release phosphate into pore waters through the breakdown of polyphosphate (Schulz and Schulz, 2005; Goldhammer et al., 2010) but also serve as templates for crystal nucleation (Cosmidis et al., 2013). The tiny CFA spheroids in the studied successions differ from large-sized euhedral apatite prisms (>100 μm) or vein fillings observed in magmatic or metamorphic systems (Bruand et al., 2019). Moreover, the Xiamaling Formation in the studied area has only experienced a low degree of thermal maturity based on pyrolysis analysis (Zhang et al., 2015). It is thus possible to use the $\delta^{18}O$ thermometer to constrain the temperature of pore water from which the CFA was precipitated.

To assess Mesoproterozoic marine temperatures, we start by considering the seawater $\delta^{18}O_w$, a key parameter controlling pore water $\delta^{18}O_w$. The $\delta^{18}O_w$ of seawater has been an intense and ongoing debate, arguing for either a stable $\delta^{18}O_w$ (Muehlenbachs, 1998) or a secular $\delta^{18}O_w$ variation over time (Jaffrés et al., 2007). Two $\delta^{18}O_w$ compositions

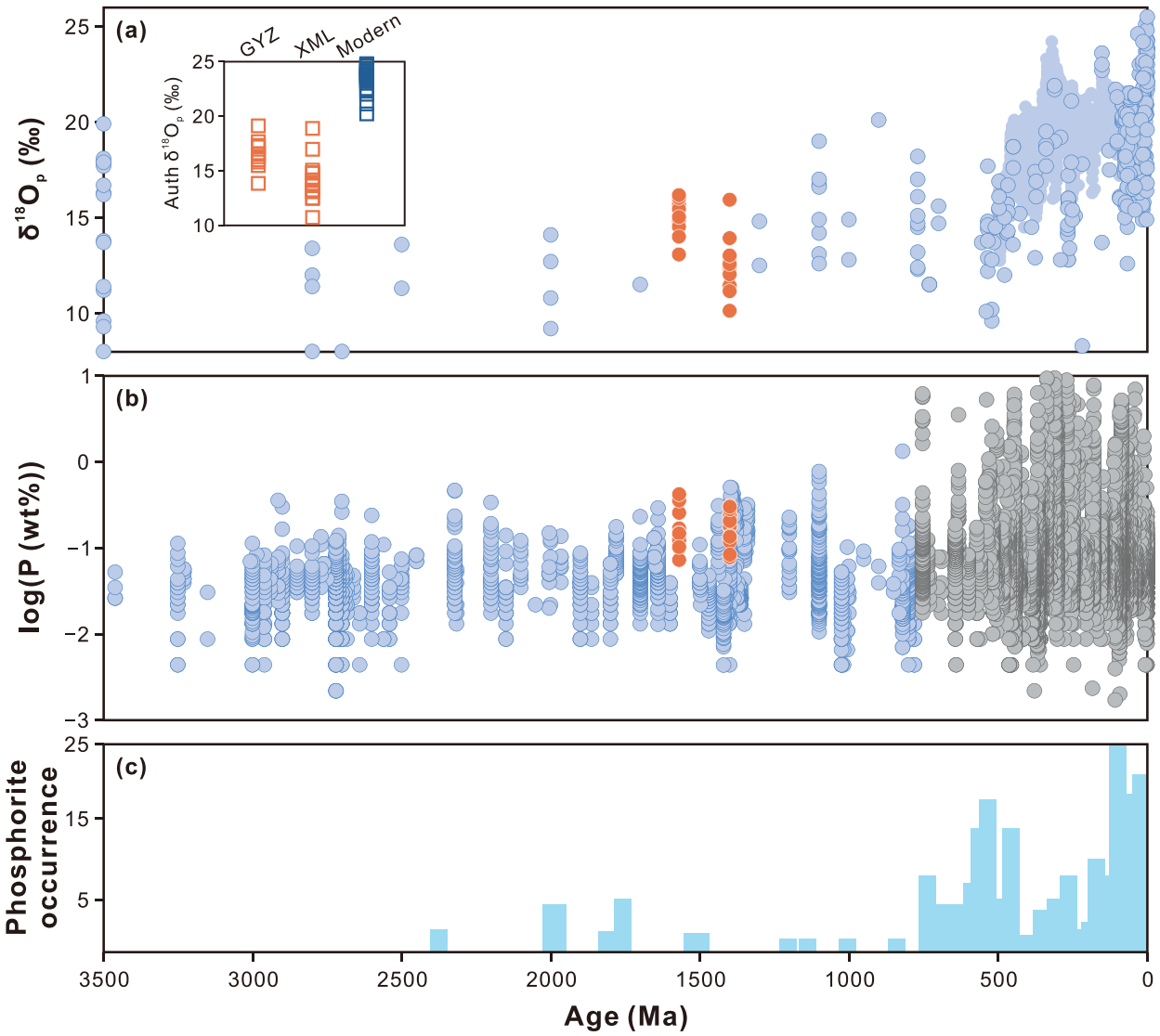

Fig. 5. Data compilation from 3.5 Ga to present day. (a) Raw $\delta^{18}O_p$ values from apatite-bearing sediments (outlined dots; Longinelli and Nuti, 1968; Karhu and Epstein, 1986; Shemesh et al., 1988; Blake et al., 2010; Sun et al., 2020; Smith et al., 2021) and from Phanerozoic phosphate fossils (dots without outlines; Grossman and Joachimski, 2022). Note that variations in analytical methods across publications may introduce potential bias when comparing these data. The inset depicts a comparison of $\delta^{18}O_{auth}$ between Mesoproterozoic and modern sediments (Jaisi and Blake, 2010). GYZ, Gaoyuzhuang Formation; XML, Xiamaling Formation. (b) Bulk P contents in shales before (blue) and after (gray) ~0.75 Ga (Planavsky et al., 2023). (C) Phosphorite occurrence over time (Reinhard et al., 2017). (For interpretation of the references to colour in this figure legend, the reader is referred to the web version of this article.)

that are relatively close to the age of our samples have been reported. One is from the ~2.4 Ga Vetreny belt rocks ($\delta^{18}O_w = -1.7‰$; Zakharov and Bindeman, 2019) and the other is from the ~760 Ma Bou Azzer ophiolite ($\delta^{18}O_w = -1.33‰$; Hodel et al., 2018). Therefore, we can assume a Mesoproterozoic $\delta^{18}O_w$ range of −1.7‰ to −1.33‰, which aligns with the oxygen-flux modelling of Herwartz et al. (2021). However, a $\delta^{18}O_w$ reconstruction based on signatures preserved in iron oxides indicated that the $\delta^{18}O_w$ of Mesoproterozoic oceans could be as low as −8‰ (Galili et al., 2019). Since we see no unique way to validate these estimates, both values are utilized in subsequent calculations.

Diagenetic processes, such as sulfate reduction and clay dewatering, can drive pore water $\delta^{18}O_w$ away from seawater $\delta^{18}O_w$ (Loyd et al., 2012). We evaluate the diagenetic influence by comparing the studied formations with sediments of the Peruvian oxygen minimum zone (OMZ), where active phosphogenesis and high flux of organic burial were detected (Ruttenberg, 2014). The depositional environment of the Xiamaling Formation is particularly similar to the Peruvian margin, as it has been demonstrated to record a Mesoproterozoic OMZ (Zhang et al., 2016; Wang et al., 2017). Investigations on the Peruvian pore waters revealed a $\delta^{18}O_w$ deviation of ~0.5‰ during early diagenesis (Kastner et al., 1990; Meister et al., 2008), which represents potential diagenetic alterations that need to be included in our calculation.

Lastly, a $\delta^{18}O_p$ in equilibrium with pore water $\delta^{18}O_w$ should be determined. The $\delta^{18}O_{auth}$ values range from 13.8‰ to 19.1‰ in the Gaoyuzhuang Formation and from 10.7‰ to 18.9‰ in the Xiamaling Formation (Fig. 4). These variations could be attributed to either temperature shift during CFA precipitation or fractionation that occurred via the hydrolysis of organic P compounds. Laboratory studies have shown that the enzymatic degradation of organic P is accompanied by incorporation of one or two oxygen atoms from water with kinetic isotope effects, producing $\delta^{18}O_p$ lower than the equilibrium composition (Liang and Blake, 2006, 2009; von Sperber et al., 2014). Given the close relationship between CFA and organic matter in our samples, organic P hydrolysis could have played an important role in both forming CFA and disrupting the $\delta^{18}O_p$ equilibrium. We use the largest $\delta^{18}O_{auth}$ to represent the equilibrium signal. Combing this value with Eq. (1) and pore

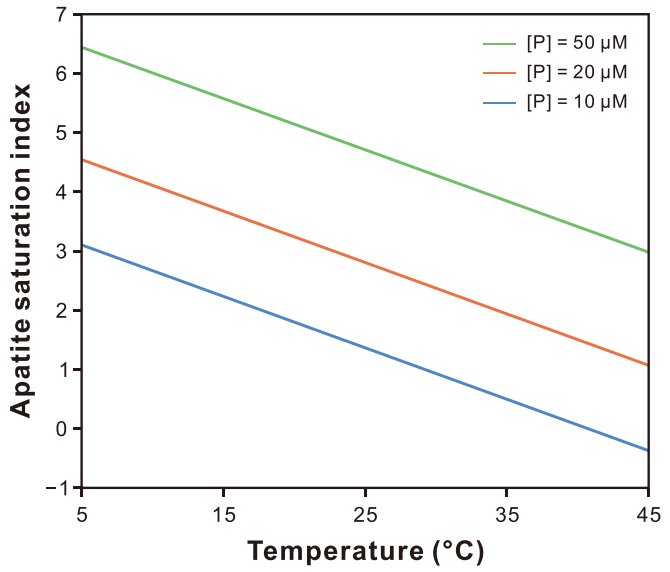

Fig. 6. Saturation states of CFA at different temperatures calculated by the PHREEQC software. There are considerable uncertainties in the estimation of ion concentrations including Ca, P, F, and others. The pH of Mesoproterozoic pore water is also underconstrained. However, reasonable changes in these parameters would not change the overall trends in saturation index.

water $\delta^{18}O_w$ of −1.7‰ to −1.33‰ (± 0.5‰) yields a temperature of 25.2 ± 8.2 °C for the Mesoproterozoic seafloor (Monte Carlo method). On the other hand, applying a $\delta^{18}O_w$ of −8 ± 0.5‰ would result in unrealistic temperature (−3.9 ± 9.2 °C). It is noteworthy that pore water $\delta^{18}O_p$ of dissolved phosphate from the Peruvian sediments could be 0–2‰ lower than the equilibrium ratio due to the superposition of biological P turnover and organic P degradation (Zhao et al., 2021). Hence, even with the highest $\delta^{18}O_{auth}$, our approach may still lead to a slight overestimation of the Mesoproterozoic temperatures.

To compare the obtained temperatures with those of the modern, we plot our data along with the $\delta^{18}O_{auth}$ from the Peruvian margin (Fig. 5a; Jaisi and Blake, 2010). As mentioned above, Our samples exhibit striking resemblances to sediments beneath the Peruvian OMZ in terms of location (low-latitude), water depth (>100–200 m), and sediment properties (enriched in P and organic matter). While these values can deviate from the isotopic equilibrium, the significant difference between the $\delta^{18}O_{auth}$ of modern and Mesoproterozoic apatite conceivably indicate a warmer condition during the Mesoproterozoic Era. Such an interpretation would be consistent with evidence indicating high levels of atmospheric carbon dioxide or other greenhouse gases at that time (Kaufman and Xiao, 2003; Kah and Riding, 2007; Liu et al., 2019).

5.3. *Implications for the phosphorite paucity*

An enigmatic feature of Mesoproterozoic successions is the suppression of phosphogenesis (Fig. 5). Previous research attributes this phenomenon to a small P reservoir and the prevalence of anoxic states in coeval oceans (Reinhard et al., 2017). Theoretically, the precipitation of CFA occurs when pore water becomes supersaturated with respect to its phosphate precursors, a process largely controlled by ion concentrations and environmental factors such as temperature and pH (Jahnke, 1984; Van Cappellen and Berner, 1991; Zhao et al., 2020; Brady et al., 2022). Our study of $\delta^{18}O_{auth}$ allows us to evaluate the temperature impact on P authigenesis. In the following, we utilize the PHREEQC program to calculate the saturation index (SI) for CFA under varying temperatures:

$$SI = log(IAP/K) \quad (4)$$

where IAP is the ion activity product, K is the solubility product. SI > 0 denotes supersaturation of the solution with respect to CFA, while SI < 0 represents unsaturation. The larger the SI, the more CFA will be precipitated.

As illustrated in Fig. 6, the SI declines with rising temperature. An increase in pore water temperature of 10 °C will induce a reduction in SI by approximately one unit, corresponding to an order of magnitude decrease in the degree of supersaturation. It is plausible that the warm Mesoproterozoic oceans could have contributed to the scarcity of phosphorite by hindering CFA precipitation, especially under a P-limited marine system. Notably, the temperature-control on CFA authigenesis may have also played a role in modulating the P cycle during the Phanerozoic Eon. For instance, anomalously high ratios of organic carbon to total P preserved in sediments of the Cretaceous oceanic anoxic events were suggested to be caused by high temperatures and consequently low rates of CFA precipitation (Papadomanolaki et al., 2022), a conclusion align with our findings.

6. Conclusions and future directions

Authigenic CFA spheroids are observed in the Gaoyuzhuang and Xiamaling samples, but the bulk P abundances are lower compared to their Phanerozoic counterparts. The calculated $\delta^{18}O_{auth}$ values likely indicate a warm climate during the Mesoproterozoic Era. Based on thermodynamic calculations, we propose that the elevated temperatures could have inhabited CFA authigenesis, partially accounting for the scarcity of phosphorite in coeval strata. However, further validation of this idea and more nuanced investigations are still warranted. Many types of sediment remain unexplored, and the Mesoproterozoic $\delta^{18}O_{auth}$ data are sparse relative to the Phanerozoic record. Refinement of $\delta^{18}O_{auth}$ could be achieved through sequential extraction or in situ microscale analysis. Additionally, the emerging field of triple oxygen isotopes offers a promising avenue for gaining deeper insights into P dynamics. Such studies hold potential not only to enhance our understanding of the P cycle, but also to shed light on the interplay between P availability and life evolution.

Declaration of Competing Interest

The authors declare that they have no known competing financial interests or personal relationships that could have appeared to influence the work reported in this paper.

Data availability

All data are listed in the supplementary material.

Acknowledgments

We thank Daniel Herwartz and three anonymous reviewers for valuable reviews. We are grateful to Hailiang Dong for editorial handling, Yong Liu for helpful discussion, and Laurence Coogan for comments on an early version of the paper. This work was supported by the National Natural Science Foundation of China (42225303, 42073016, and 42102146), the National Key Research and Development Program of China (2022YFF0800304 and 2021YFA0718200), and the Villum Foundation (16518).

Appendix A. Supplementary data

Supplementary data to this article can be found online at https://doi.org/10.1016/j.chemgeo.2023.121831.

References

Algeo, T.J., Ingall, E., 2007. Sedimentary C_{org}:P ratios, paleocean ventilation, and Phanerozoic atmospheric pO_2. Palaeogeogr. Palaeoclimatol. Palaeoecol. 256, 130–155.

Bjerrum, C.J., Canfield, D.E., 2002. Ocean productivity before about 1.9 Gyr ago limited by phosphorus adsorption onto iron oxides. Nature 417, 159–162.

Blake, R.E., O'Neil, J.R., Surkov, A.V., 2005. Biogeochemical cycling of phosphorus: Insights from oxygen isotope effects of phosphoenzymes. Am. J. Sci. 305, 596–620.

Blake, R.E., Chang, S.J., Lepland, A., 2010. Phosphate oxygen isotopic evidence for a temperate and biologically active Archaean Ocean. Nature 464, 1029–1032.

Brady, M.P., Tostevin, R., Tosca, N.J., 2022. Marine phosphate availability and the chemical origins of life on Earth. Nat. Commun. 13, 5162.

Broom-Fendley, S., Heaton, T., Wall, F., Gunn, G., 2016. Tracing the fluid source of heavy REE mineralisation in carbonatites using a novel method of oxygen-isotope analysis in apatite: the example of Songwe Hill, Malawi. Chem. Geol. 440, 275–287.

Bruand, E., Storey, C., Fowler, M., Heilimo, E., 2019. Oxygen isotopes in titanite and apatite, and their potential for crustal evolution research. Geochim. Cosmochim. Acta 255, 144–162.

Canfield, D.E., Bjerrum, C.J., Zhang, S., Wang, H., Wang, X., 2020. The modern phosphorus cycle informs interpretations of Mesoproterozoic Era phosphorus dynamics. Earth-Sci. Rev. 208, 103267.

Chang, S.J., Blake, R.E., Colman, A.S., 2021. Oxygen isotope exchange rates between phosphate and water catalyzed by inorganic pyrophosphatase: Implications for the biogeochemical cycle of phosphorus. Earth Planet. Sci. Lett. 570, 117071.

Chen, Z.-G., Yin, X.-J., Zhou, Y., 2015. Effects of GC temperature and carrier gas flow rate on on-line oxygen isotope measurement as studied by on-column CO injection. J. Mass Spectrom. 50, 1023–1030.

Colman, A.S., Blake, R.E., Karl, D.M., Fogel, M.L., Turekian, K.K., 2005. Marine phosphate oxygen isotopes and organic matter remineralization in the oceans. Proc. Natl. Acad. Sci. U. S. A. 102, 13023–13028.

Conway, C.M., Taylor, H.P., 1969. O^{18}/O^{16} and C^{13}/C^{12} ratios of coexisting minerals in the Oka and Magnet Cove carbonatite bodies. J. Geol. 77, 618–626.

Cosmidis, J., Benzerara, K., Gheerbrant, E., Estève, I., Bouya, B., Amaghzaz, M., 2013. Nanometer-scale characterization of exceptionally preserved bacterial fossils in Paleocene phosphorites from Ouled Abdoun (Morocco). Geobiology 11, 139–153.

Crockford, P., Halevy, I., 2022. Questioning the paradigm of a phosphate-limited Archean biosphere. Geophys. Res. Lett. 49 e2022GL099818.

Davies, C.L., Surridge, B.W.J., Gooddy, D.C., 2014. Phosphate oxygen isotopes within aquatic ecosystems: Global data synthesis and future research priorities. Sci. Total Environ. 496, 563–575.

Faul, K.L., Paytan, A., Delaney, M.L., 2005. Phosphorus distribution in sinking oceanic particulate matter. Mar. Chem. 97, 307–333.

Galili, N., Shemesh, A., Yam, R., Brailovsky, I., Sela-Adler, M., Schuster, E.M., Collom, C., Bekker, A., Planavsky, N., Macdonald, F.A., Préat, A., Rudmin, M., Trela, W., Sturesson, U., Heikoop, J.M., Aurell, M., Ramajo, J., Halevy, I., 2019. The geologic history of seawater oxygen isotopes from marine iron oxides. Science 365, 469–473.

Gao, L.Z., Zhang, C.H., Shi, X.Y., Zhou, H.R., Wang, Z.Q., 2007. Zircon SHRIMP U-Pb dating of the tuff bed in the Xiamaling Formation of the Qingbaikouan System in North China. Geol. Bull. China 26, 249–255 (in Chinese with English abstract).

Gao, L.Z., Zhang, C.H., Shi, X.Y., Song, B., Wang, Z.Q., Liu, Y.M., 2008a. Mesoproterozoic age for Xiamaling Formation in North China Plate indicated by zircon SHRIMP dating. Chin. Sci. Bull. 53, 2665–2671.

Gao, L.Z., Zhang, C.H., Yin, C.Y., Shi, X.Y., Wang, Z.Q., Liu, Y.M., Liu, P.J., Tang, F., Song, B., 2008b. SHRIMP zircon ages: Basis for refining the chronostratigraphic classification of the Meso- and Neoproterozoic strata in North China Old Land. Acta Geosci. Sin. 29, 366–376 (in Chinese with English abstract).

Goldhammer, T., Brüchert, V., Ferdelman, T.G., Zabel, M., 2010. Microbial sequestration of phosphorus in anoxic upwelling sediments. Nat. Geosci. 3, 557–561.

Grossman, E.L., Joachimski, M.M., 2022. Ocean temperatures through the Phanerozoic reassessed. Sci. Rep. 12, 8938.

Herwartz, D., Pack, A., Nagel, T.J., 2021. A CO_2 greenhouse efficiently warmed the early Earth and decreased seawater $^{18}O/^{16}O$ before the onset of plate tectonics. Proc. Natl. Acad. Sci. U. S. A. 118, e2023617118.

Hodel, F., Macouin, M., Trindade, R.I.F., Triantafyllou, A., Ganne, J., Chavagnac, V., Berger, J., Rospabé, M., Destrigneville, C., Carlut, J., Ennih, N., Agrinier, P., 2018. Fossil black smoker yields oxygen isotopic composition of Neoproterozoic seawater. Nat. Commun. 9, 1453.

Ingalls, M., Grotzinger, J.P., Present, T., Rasmussen, B., Fischer, W.W., 2022. Carbonate-associated phosphate (CAP) indicates elevated phosphate availability in Neoarchean shallow marine environments. Geophys. Res. Lett. 49 e2022GL098100.

Jaffrés, J.B.D., Shields, G.A., Wallmann, K., 2007. The oxygen isotope evolution of seawater: a critical review of a long-standing controversy and an improved geological water cycle model for the past 3.4 billion years. Earth-Sci. Rev. 83, 83–122.

Jahnke, R.A., 1984. The synthesis and solubility of carbonate fluorapatite. Am. J. Sci. 284, 58–78.

Jaisi, D.P., Blake, R.E., 2010. Tracing sources and cycling of phosphorus in Peru margin sediments using oxygen isotopes in authigenic and detrital phosphates. Geochim. Cosmochim. Acta 74, 3199–3212.

Jones, C., Nomosatryo, S., Crowe, S.A., Bjerrum, C.J., Canfield, D.E., 2015. Iron oxides, divalent cations, silica, and the early earth phosphorus crisis. Geology 43, 135–138.

Kah, L.C., Riding, R., 2007. Mesoprotezoic carbon dioxide levels inferred from calcified cyanobacteria. Geology 35, 799–802.

Karhu, J., Epstein, S., 1986. The implication of the oxygen isotope records in coexisting cherts and phosphates. Geochim. Cosmochim. Acta 50, 1745–1756.

Kastner, M., Elderfield, H., Martin, J.B., Suess, Erwin, Kvenvolden, K.A., Garrison, R.E., 1990. Diagenesis and interstitial-water chemistry at the Peruvian continental margin — major constituents and strontium isotopes. In: Suess, E., von Huene, R. (Eds.), Proceedings of the Ocean Drilling Program. Scientific Results, pp. 413–440.

Kaufman, A.J., Xiao, S., 2003. High CO_2 levels in the Proterozoic atmosphere estimated from analyses of individual microfossils. Nature 425, 279–282.

Lécuyer, C., Amiot, R., Touzeau, A., Trotter, J., 2013. Calibration of the phosphate $\delta^{18}O$ thermometer with carbonate-water oxygen isotope fractionation equations. Chem. Geol. 347, 217–226.

Lei, X.-T., Zhang, H., Chen, M., Guo, L., Zhang, X.-G., Jiang, Z.-H., Blake, R.E., Chen, Z.-G., 2020. The efficiency of sequential extraction of phosphorus in soil and sediment: insights from the oxygen isotope ratio of phosphate. J. Soils Sediments 20, 1332–1343.

Li, H.K., Zhu, S.X., Xiang, Z.Q., Su, W.B., Lu, S.N., Zhou, H.Y., Geng, J.Z., Li, S., Yang, F. J., 2010. Zircon U-Pb dating on tuff bed from Gaoyuzhuang Formation in Yanqing, Beijing: further constraints on the new subdivision of the Mesoproterozoic stratigraphy in the northern North China Craton. Acta Petrol. Sin. 26, 2131–2140 (in Chinese with English abstract).

Li, Z., Xi, S., Hu, J., Dong, X., Zhang, G., 2019. New insights about the Mesoproterozoic sedimentary framework of North China Craton. Geol. J. 54, 409–425.

Liang, Y., Blake, R.E., 2006. Oxygen isotope signature of P_i regeneration from organic compounds by phosphomonoesterases and photooxidation. Geochim. Cosmochim. Acta 70, 3957–3969.

Liang, Y., Blake, R.E., 2007. Oxygen isotope fractionation between apatite and aqueous-phase phosphate: 20–45 °C. Chem. Geol. 238, 121–133.

Liang, Y., Blake, R.E., 2009. Compound- and enzyme-specific phosphodiester hydrolysis mechanisms revealed by $\delta^{18}O$ of dissolved inorganic phosphate: Implications for marine P cycling. Geochim. Cosmochim. Acta 73, 3782–3794.

Liu, P., Liu, Y., Hu, Y., Yang, J., Pisarevsky, S.A., 2019. Warm climate in the "Boring billion" era. Acta Geol. Sin. 93, 40–43.

Longinelli, A., Nuti, S., 1968. Oxygen isotopic composition of phosphorites from marine formations. Earth Planet. Sci. Lett. 5, 13–16.

Loyd, S.J., Corsetti, F.A., Eiler, J.M., Tripati, A.K., 2012. Determining the diagenetic conditions of concretion formation: Assessing temperatures and pore waters using clumped isotopes. J. Sediment. Res. 82, 1006–1016.

McLaughlin, K., Sohm, J.A., Cutter, G.A., Lomas, M.W., Paytan, A., 2013. Phosphorus cycling in the Sargasso Sea: Investigation using the oxygen isotopic composition of phosphate, enzyme-labeled fluorescence, and turnover times. Glob. Biogeochem. Cycles 27, 375–387.

Meister, P., Bernasconi, S.M., Vasconcelos, C., McKenzie, J.A., 2008. Sealevel changes control diagenetic dolomite formation in hemipelagic sediments of the Peru margin. Mar. Geol. 252, 166–173.

Meng, Q.-R., Wei, H.-H., Qu, Y.-Q., Ma, S.-X., 2011. Stratigraphic and sedimentary records of the rift to drift evolution of the northern North China craton at the Paleo- to Mesoproterozoic transition. Gondwana Res. 20, 205–218.

Mizota, C., Domon, Y., Yoshida, N., 1992. Oxygen isotope composition of natural phosphates from volcanic ash soils of the Great Rift Valley of Africa and East Java, Indonesia. Geoderma 53, 111–123.

Muehlenbachs, K., 1998. The oxygen isotopic composition of the oceans, sediments and the seafloor. Chem. Geol. 145, 263–273.

Papadomanolaki, N.M., Lenstra, W.K., Wolthers, M., Slomp, C.P., 2022. Enhanced phosphorus recycling during past oceanic anoxia amplified by low rates of apatite authigenesis. Sci. Adv. 8, eabn2370.

Papineau, D., 2010. Global biogeochemical changes at both ends of the Proterozoic: Insights from phosphorites. Astrobiology 10, 165–181.

Planavsky, N.J., Asael, D., Rooney, A.D., Robbins, L.J., Gill, B.C., Dehler, C.M., Cole, D. B., Porter, S.M., Love, G.D., Konhauser, K.O., Reinhard, C.T., 2023. A sedimentary record of the evolution of the global marine phosphorus cycle. Geobiology 21, 168–174.

Qu, Y., Pan, J., Ma, S., Lei, Z., Li, L., Wu, G., 2014. Geological characteristics and tectonic significance of unconformities in Mesoproterozoic successions in the northern margin of the North China Block. Geosci. Front. 5, 127–138.

Rasmussen, B., Muhling, J.R., Suvorova, A., Fischer, W.W., 2021. Apatite nanoparticles in 3.46–2.46 Ga iron formations: evidence for phosphorus-rich hydrothermal plumes on early Earth. Geology 49, 647–651.

Reinhard, C.T., Planavsky, N.J., Gill, B.C., Ozaki, K., Robbins, L.J., Lyons, T.W., Fischer, W.W., Wang, C., Cole, D.B., Konhauser, K.O., 2017. Evolution of the global phosphorus cycle. Nature 541, 386–389.

Rudnick, R.L., Gao, S., 2014. Composition of the continental crust. In: Holland, H.D., Turekian, K.K. (Eds.), Treatise on Geochemistry. Elsevier, pp. 1–51.

Ruttenberg, K.C., 2014. The global phosphorus cycle. In: Holland, H.D., Turekian, K.K. (Eds.), Treatise on Geochemistry. Elsevier, pp. 499–558.

Schulz, H.N., Schulz, H.D., 2005. Large sulfur bacteria and the formation of phosphorite. Science 307, 416–418.

Shemesh, A., Kolodny, Y., Luz, B., 1988. Isotope geochemistry of oxygen and carbon in phosphate and carbonate of phosphorite francolite. Geochim. Cosmochim. Acta 52, 2565–2572.

Smith, A.C., Pfahler, V., Tamburini, F., Blackwell, M.S.A., Granger, S.J., 2021. A review of phosphate oxygen isotope values in global bedrocks: Characterising a critical endmember to the soil phosphorus system. J. Plant Nutr. Soil Sci. 184, 25–34.

Stow, D.A.V., Huc, A.-Y., Bertrand, P., 2001. Depositional processes of black shales in deep water. Mar. Pet. Geol. 18, 491–498.

Su, W., Zhang, S., Huff, W.D., Li, H., Ettensohn, F.R., Chen, X., Yang, H., Han, Y., Song, B., Santosh, M., 2008. SHRIMP U-Pb ages of K-bentonite beds in the Xiamaling Formation: Implications for revised subdivision of the Meso- to Neoproterozoic history of the North China Craton. Gondwana Res. 14, 543–553.

Su, W.B., Li, H.K., Huff, W.D., Ettensohn, F.R., Zhang, S.H., Zhou, H.Y., Wan, Y.S., 2010. SHRIMP U-Pb dating for a K-bentonite bed in the Tieling Formation, North China. Chin. Sci. Bull. 55, 3312–3323.

Sun, Y., Amelung, W., Wu, B., Haneklaus, S., Maekawa, M., Lücke, A., Schnug, E., Bol, R., 2020. 'Co-evolution' of uranium concentration and oxygen stable isotope in phosphate rocks. Appl. Geochem. 114, 104476.

Syverson, D.D., Reinhard, C.T., Isson, T.T., Holstege, C.J., Katchinoff, J.A.R., Tutolo, B. M., Etschmann, B., Brugger, J., Planavsky, N.J., 2021. Nutrient supply to planetary biospheres from anoxic weathering of mafic oceanic crust. Geophys. Res. Lett. 48 e2021GL094442.

Tamburini, F., Pfahler, V., Bünemann, E.K., Guelland, K., Bernasconi, S.M., Frossard, E., 2012. Oxygen isotopes unravel the role of microorganisms in phosphate cycling in soils. Environ. Sci. Technol. 46, 5956–5962.

Tian, L., Guo, Q., Zhu, Y., He, H., Lang, Y., Hu, J., Zhang, H., Wei, R., Han, X., Peters, M., Yang, J., 2016. Research and application of method of oxygen isotope of inorganic phosphate in Beijing agricultural soils. Environ. Sci. Pollut. Res. 23, 23406–23414.

Tian, H., Li, H.K., Zhang, J., Su, W.B., Liu, H., Xiang, Z.Q., Zhong, Y., 2020. SHRIMP U-Pb dating for zircons from the tuff bed of the Mesoproterozoic Gaoyuzhuang Formation in Jixian Section, Tianjin, and its constraints on the Mesoproterozoic bio-environmental events. Geol. Surv. Res. 43, 153–160 (in Chinese with English abstract).

Tichomirowa, M., Grosche, G., Götze, J., Belyatsky, B.V., Savva, E.V., Keller, J., Todt, W., 2006. The mineral isotope composition of two Precambrian carbonatite complexes from the Kola Alkaline Province – Alteration versus primary magmatic signatures. Lithos 91, 229–249.

Van Cappellen, P., Berner, R.A., 1991. Fluorapatite crystal growth from modified seawater solutions. Geochim. Cosmochim. Acta 55, 1219–1234.

Van Cappellen, P., Ingall, E.D., 1996. Redox stabilization of the atmosphere and oceans by phosphorus-limited marine productivity. Science 271, 493–496.

von Sperber, C., Kries, H., Tamburini, F., Bernasconi, S.M., Frossard, E., 2014. The effect of phosphomonoesterases on the oxygen isotope composition of phosphate. Geochim. Cosmochim. Acta 125, 519–527.

Walton, C.R., Hao, J., Huang, F., Jenner, F.E., Williams, H., Zerkle, A.L., Lipp, A., Hazen, R.M., Peters, S.E., Shorttle, O., 2023. Evolution of the crustal phosphorus reservoir. Sci. Adv. 9, eade6923.

Wang, X., Zhang, S., Wang, H., Bjerrum, C.J., Hammarlund, E.U., Haxen, E.R., Su, J., Wang, Y., Canfield, D.E., 2017. Oxygen, climate and the chemical evolution of a 1400 million year old tropical marine setting. Am. J. Sci. 317, 861–900.

Ye, Y., Zhang, S., Wang, H., Wang, X., Tan, C., Li, M., Wu, C., Canfield, D.E., 2021. Black shale Mo isotope record reveals dynamic ocean redox during the Mesoproterozoic Era. Geochem. Perspect. Lett. 18, 16–21.

Ye, Y., Wang, H., Wang, X., Li, J., Wu, C., Zhang, S., 2023. Regional and global proxies for varying ocean redox conditions at ~1.57 Ga: a causal connection with volcanism-induced weathering. Geosyst. Geoenviron. 2, 100173.

Zakharov, D.O., Bindeman, I.N., 2019. Triple oxygen and hydrogen isotopic study of hydrothermally altered rocks from the 2.43–2.41 Ga Vetreny belt, Russia: an insight into the early Paleoproterozoic seawater. Geochim. Cosmochim. Acta 248, 185–209.

Zhai, M., Hu, B., Zhao, T., Peng, P., Meng, Q., 2014. Late Paleoproterozoic-Neoproterozoic multi-rifting events in the North China Craton and their geological significance: a study advance and review. Tectonophysics 662, 153–166.

Zhang, S., Li, Z.-X., Evans, D.A.D., Wu, H., Li, H., Dong, J., 2012. Pre-Rodinia supercontinent Nuna shaping up: a global synthesis with new paleomagnetic results from North China. Earth Planet. Sci. Lett. 353–354, 145–155.

Zhang, S., Wang, X., Hammarlund, E.U., Wang, H., Costa, M.M., Bjerrum, C.J., Connelly, J.N., Zhang, B., Bian, L., Canfield, D.E., 2015. Orbital forcing of climate 1.4 billion years ago. Proc. Natl. Acad. Sci. U. S. A. 112, E1406–E1413.

Zhang, S., Wang, X., Wang, H., Bjerrum, C.J., Hammarlund, E.U., Costa, M.M., Connelly, J.N., Zhang, B., Su, J., Canfield, D.E., 2016. Sufficient oxygen for animal respiration 1,400 million years ago. Proc. Natl. Acad. Sci. U. S. A. 113, 1731–1736.

Zhang, S., Chang, L., Zhao, H., Ding, J., Xian, H., Li, H., Wu, H., Yang, T., 2021. The Precambrian drift history and paleogeography of the Chinese cratons. In: Pesonen, L. J., Salminen, J., Elming, S.-Å., Evans, D.A.D., Veikkolainen, T. (Eds.), Ancient Supercontinents and the Paleogeography of Earth. Elsevier, pp. 333–376.

Zhao, M., Zhang, S., Tarhan, L.G., Reinhard, C.T., Planavsky, N., 2020. The role of calcium in regulating marine phosphorus burial and atmospheric oxygenation. Nat. Commun. 11, 2232.

Zhao, M., Blake, R.E., Liang, Y., Ruf, D.D., Jaisi, D.P., Chang, S.J., Planavsky, N.J., 2021. Oxygen isotopic fingerprints on the phosphorus cycle within the deep subseafloor biosphere. Geochim. Cosmochim. Acta 310, 169–186.